

## Article

# Investigating the Intrinsic Anisotropy of VO<sub>2</sub>(101) Thin Films Using Linearly Polarized Resonant Photoemission Spectroscopy

Alessandro D'Elia <sup>1,2,\*</sup>, Vincent Polewczyk <sup>3</sup>, Aleksandr Yu. Petrov <sup>3</sup>, Liang Li <sup>4</sup>, Chongwen Zou <sup>4</sup>, Javad Rezvani <sup>3,5</sup> and Augusto Marcelli <sup>1,2,6</sup>

<sup>1</sup> CNR–Istituto Struttura della Materia, Basovizza Area Science Park, 34149 Trieste, Italy

<sup>2</sup> Rome International Center for Materials Science Superstripes RICMASS, Via dei Sabelli 119A, 00185 Roma, Italy

<sup>3</sup> Laboratorio TASC, Istituto Officina dei Materiali (IOM)–CNR, Area Science Park, S.S.14, km 163.5, 34149 Trieste, Italy

<sup>4</sup> National Synchrotron Radiation Laboratory, University of Science and Technology of China, Hefei 230029, China

<sup>5</sup> Scuola di Scienze e Tecnologie, Sezione di Fisica, Università di Camerino, Via Madonna delle Carceri 9, 62032 Camerino, Italy

<sup>6</sup> Laboratori Nazionali di Frascati, Istituto Nazionale di Fisica Nucleare, 00044 Frascati, Italy

\* Correspondence: alessandro.delia@lnf.infn.it

**Abstract:** VO<sub>2</sub> is one of the most studied vanadium oxides because it undergoes a reversible metal-insulator transition (MIT) upon heating with a critical temperature of around 340 K. One of the most overlooked aspects of VO<sub>2</sub> is the band's anisotropy in the metallic phase when the Fermi level is crossed by two bands:  $\pi^*$  and  $d_{||}$ . They are oriented perpendicularly in one respect to the other, hence generating anisotropy. One of the parameters tuning MIT properties is the unbalance of the electron population of  $\pi^*$  and  $d_{||}$  bands that arise from their different energy position with respect to the Fermi level. In systems with reduced dimensionality, the electron population disproportion is different with respect to the bulk leading to a different anisotropy. Investigating such a system with a band-selective spectroscopic tool is mandatory. In this manuscript, we show the results of the investigation of a single crystalline 8 nm VO<sub>2</sub>/TiO<sub>2</sub>(101) film. We report on the effectiveness of linearly polarized resonant photoemission (ResPES) as a band-selective technique probing the intrinsic anisotropy of VO<sub>2</sub>.

**Keywords:** VO<sub>2</sub>; metal insulator transition; bands anisotropy; resonant photoemission; electron correlation; strained films



**Citation:** D'Elia, A.; Polewczyk, V.; Petrov, A.Y.; Li, L.; Zou, C.; Rezvani, J.; Marcelli, A. Investigating the Intrinsic Anisotropy of VO<sub>2</sub>(101) Thin Films Using Linearly Polarized Resonant Photoemission Spectroscopy. *Condens. Matter* **2023**, *8*, 40. <https://doi.org/10.3390/condmat8020040>

Academic Editors: Krzysztof Wohlfeld and Atsushi Fujimori

Received: 19 December 2022

Revised: 17 April 2023

Accepted: 20 April 2023

Published: 26 April 2023



**Copyright:** © 2023 by the authors. Licensee MDPI, Basel, Switzerland. This article is an open access article distributed under the terms and conditions of the Creative Commons Attribution (CC BY) license (<https://creativecommons.org/licenses/by/4.0/>).

## 1. Introduction

Vanadium oxides are an extremely interesting class of materials that are mostly studied for their reversible metal-to-insulator transition (MIT) [1–7]. Among them, one of the most studied is VO<sub>2</sub>. The transition temperature is close to room temperature (about 340 K in bulk VO<sub>2</sub>), and a large jump in resistivity [8,9] makes this material extremely appealing for applications such as energy saving [10–12], new-generation electronic devices based on electron correlation and ultra-fast switching [13–15]. The nature of the MIT itself has been the grounds of a long debate because of the simultaneous presence of a structural phase transition and a MIT (VO<sub>2</sub> passes from a monoclinic insulator to a metallic metal upon heating), rousing discussion about whether the VO<sub>2</sub> MIT could be classified as a Mott or a Peierls transition [2,16–19]. Despite the ongoing debate, experimental evidence has shown that VO<sub>2</sub> MIT can be controlled by the interplay among electronic, orbital, and lattice degrees of freedom [9,18,20–24]. MIT has been the grounds of great interest because VO<sub>2</sub> belongs to a class of transition–metal complexes known as correlated intermediate valent systems, including lanthanides [25–27]. In these systems, the electron wavefunctions

in the metal and ligand orbitals near the Fermi level both possess similar energies but with a small-to-zero overlap due to the Coulomb repulsion. Even with a small overlap, electrons have similar probabilities of being found on one or on the other site because of the existing configuration interaction between multiple possible electronic configurations, in which the redox state of the metal is different [28,29].

In this scenario, strain emerged as a powerful method to control the MIT, and VO<sub>2</sub>-strained films have been deeply studied [9,23,30–36]. Since strains modify interatomic distances changing the vanadium-oxygen overlap, the orbital energy hierarchy needs to be considered, and, in the last analysis, the bands' population at the Fermi level (FL).

Moreover, the metallic phase of VO<sub>2</sub> is strongly anisotropic [36–39]. This often is an overseen aspect that has to be taken into account for a complete understanding of the MIT mechanism.

The metallic phase of VO<sub>2</sub> has tetragonal lattice symmetry with main axis *a*, *b*, and *c* (see Figure 1). In this phase, FL is crossed by the bands  $\pi^*$  and  $d_{||}$  [40]. The  $\pi^*$  band is generated by the overlap of antibonding O *2p* electrons with V *3d* electrons lying in the *a*-*b* plane while the  $d_{||}$  is composed of unpaired V *3d* electrons and is oriented along the *c* axis. The intrinsic anisotropy of metallic VO<sub>2</sub> arises from the orientation of  $\pi^*$  and  $d_{||}$  which are oriented perpendicularly, one with respect to the other [5,23,40].

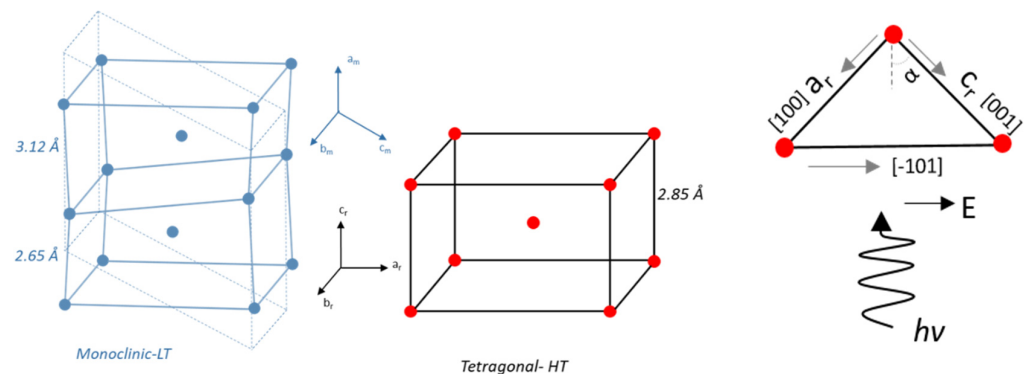


**Figure 1.** (Left): Sketch of the low temperature (LT) monoclinic insulator lattice (continuous line) and unit cell (broken line). (Center): Sketch of the tetragonal high temperature (HT) metal lattice unit cell. For both insulating and metallic phases full circles represent vanadium atoms. (Right): Top view of the lattice parameters orientation when the sample is oriented in normal incidence geometry, i.e.,  $h\nu$  propagation direction parallel to (101).

The  $\pi^*$  and  $d_{||}$  bands are not equally occupied, with the  $\pi^*$  band appearing typically less populated with respect to the  $d_{||}$  band. This unbalance is generated by their different energy position with respect to FL, as explained by Goodenough in his pivotal work [40]. The disproportion in electron population is a key parameter to control the MIT since it is proportional to the electron correlation experienced by V *3d* electrons [23,31,41,42]. This unbalanced electron population can be tuned by strain [23,41], thus influencing the band anisotropy of VO<sub>2</sub>. Although discriminating the individual contribution of the  $\pi^*$  and  $d_{||}$  bands is very important in VO<sub>2</sub>, isolating the contribution from one of these bands is hard when employing standard spectroscopic techniques. Using a band selective and chemical selective method is, thus, of paramount importance to obtain insights into the MIT mechanism.

In this manuscript, we reported our investigation of the intrinsic band structure anisotropy of a single crystalline 8 nm VO<sub>2</sub>/TiO<sub>2</sub>(101) film using a linearly polarized resonant photoemission spectroscopy (ResPES) in order to maximally enhance the orbital selectivity and the photoemission yield.

As we demonstrated in our previous work, this technique allowed us to study the orbital contribution that VO<sub>2</sub> thin films have on MIT [33,34,41,43]. Combining this approach with linear polarization, we obtained the ideal band selective probe for VO<sub>2</sub> intrinsic

anisotropy. Orienting the electric field vector  $E$  of the incident photon beam along the  $c$ -axis of the metallic phase ( $c_r$ ), the contribution from the  $d_{||}$  band to the ResPES spectra was maximum. On the other hand, when  $E$  was parallel to  $a_r$  (thus, perpendicular to  $c_r$ ), sensitivity to the  $\pi^*$  band was maximum [44]. Our experimental results show how the use of linearly polarized ResPES is critical in order to study the anisotropy of  $\text{VO}_2$  and the contribution of the different bands populating FL to MIT.

## 2. Experimental

The 8 nm  $\text{VO}_2$  thick film was deposited on a clean substrate of  $\text{TiO}_2$  (101) using RF-plasma-assisted oxide-MBE. The base pressure in the deposition chamber was  $<4 \times 10^{-9}$  mbar. The film thickness was controlled by monitoring the deposition time and using a growth rate of 0.1 Å/s. The substrate was heated at a temperature of 550 °C during the deposition. More detailed information on epitaxial film preparation has been reported elsewhere [9,45].

The sample has been characterized using X-ray diffraction (XRD) and resistivity measurements. XRD measurements were performed using a PanAnalytical X'Pert Pro diffractometer (Cu- $K\alpha$  wavelength). The resistivity measurements were carried out using the Van der Pauw method.

The ResPES and X-ray absorption (XAS) measurements were performed at the NFFA APE-HE beamline at the Elettra synchrotron radiation facility [46]. XAS measurements were acquired in the total electron yield (TEY) at the  $V L_3$  edge at RT and at about 353 K. The light polarization was set to horizontal for all the measurements. ResPES measurements were taken with a Scienta R3000 hemispherical electron energy analyzer spanning the photon energy across the  $V L_3$  edge. More information about the ResPES technique can be found in Appendix A. The energy resolution for XAS was 0.1 eV, while for ResPES measurements, it was 200 meV. The photoelectron's binding energies were calibrated with respect to the Fermi level of a gold reference foil. The sample surface was treated with mild annealing (120 °C, for 50 min) in UHV conditions in order to remove part of the contaminants. A higher temperature was not used in order to reduce the risk of altering the film stoichiometry. The use of the sputtering procedure was also avoided to minimize the risk of inadvertently reducing the film thickness. These limitations had the overall effect of leaving some residual contaminants on the sample surface, which, nevertheless, was not enough to compromise our measurements.

The metallic  $\text{VO}_2$  lattice parameters orientation for ResPES and XAS acquisitions are reported in Figure 1.

In order to align the electric field vector of the incident photon beam along the two main axes,  $c_r$  and  $a_r$ , the sample was rotated to an angle  $\alpha = \pm 45$ . In this configuration, we calculated (using the lattice parameters reported in JCPDS no. 76-0675) an effective angle between the electric field vector and the  $a$  and  $c$  axis of about  $13^\circ$ . This did not influence our band sensitivity since it depended on the square cosine of the angle occurring between the target band end of the incident electric field [47]. In our case  $\cos^2(13^\circ)$  was  $\sim 0.95$ , which meant that our measurements had 95% of the band's sensitivity with respect to the ideal case in which the incident electric field and orbital orientations were perfectly aligned.

## 3. Results and Discussion

The 8 nm  $\text{VO}_2$  thick film quality was checked using XRD, and resistivity measurements are reported in Figure 2. The resistivity hysteresis showed a large jump of about three orders of magnitude, pointing out the good quality of the film. The critical temperature  $T_c$  and the width of transition  $\Delta T$  were 321 and 8.2 K, respectively, which is in good agreement with similar films investigated in the literature [35,48]. The  $T_c$  was calculated as the average temperature between the two minima of  $\frac{\partial \log \rho}{\partial T}$ .

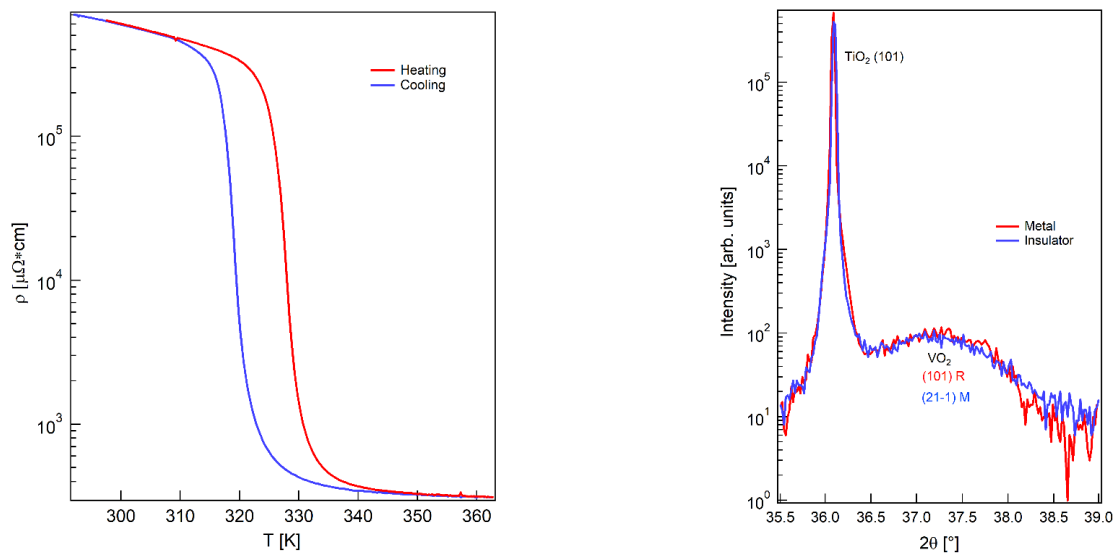


**Figure 2.** (Left): Resistivity hysteresis of the 8 nm  $\text{VO}_2/\text{TiO}_2(101)$  film. (Right): XRD pattern of the  $\text{VO}_2/\text{TiO}_2(101)$  film in the metallic (red line, acquired at 338.15 K) and insulating (blue line, acquired at room temperature) phases. The  $\text{VO}_2$  Miller indexes for the metallic phases are labeled by the letter R and for the insulating phase by the letter M.

The XRD patterns of the insulating and metallic phases are reported in the right panel of Figure 2. The sharp  $\text{TiO}_2(101)$  peak is clearly visible at  $\sim 36.1^\circ$ . The signal from the  $\text{VO}_2$  film is wide and centered around  $\sim 37.35^\circ$  in both phases. The shape of the  $\text{VO}_2$  peak points out that the residual strain imposed by the substrate heavily affected the  $\text{VO}_2$  lattice, which is in qualitative agreement with similar measurements performed on  $\text{VO}_2/\text{TiO}_2(101)$  thin films [35]. Since the XRD peak was so large, it was hard to exactly locate the peak's position. For the metallic phase, we were able to locate the peak at about  $\sim 37.35^\circ$ , corresponding to  $d_{101} = 1.269 \text{ \AA}$ . The value reported in JCPDS no. 76-0675 for the (101) interplanar distance for bulk  $\text{VO}_2$  was  $d_{101} = 1.277 \text{ \AA}$ , revealing the presence of a compressive strain of  $\sim 0.8\%$  along the (101) direction. In addition, the XRD patterns revealed that the film was single crystalline since no other  $\text{VO}_2$  peaks could be observed.

The band anisotropy was investigated using ResPES (acquired with photon energy tuned on the maximum of the  $V L_3$  edge) and by orienting the sample in order to obtain  $E \parallel c_r$  and  $E \perp c_r$  ( $E \parallel a_r$ ). With these two configurations, we maximized the signal coming from the  $d_{\parallel}$  and  $\pi^*$  bands, respectively. The ResPES spectra are reported in Figure 3's left panel and are qualitatively similar to previous ResPES works [43,49]. All spectra are characterized by a photoemission peak centered around 7 eV, which was generated by the overlap of  $V 3d$  and  $O 2p$  electrons, and a structure centered around 1.7 eV coming from the unpaired  $V 3d$  electrons [50]. The only exception is the off-resonance spectrum, for which the  $V 3d$  unpaired signal was too weak to be below our detection threshold, most likely due to the residual contaminants on the sample surface. This may be due to the nature of our ex-situ experiment and the experimental constraints used to clean the sample surface. This strongly suggests the necessity to access the resonant condition to enhance the signal coming from the  $V 3d$  electrons and, thus, properly study the bands around FL. In the monoclinic insulator phase, the spectra were acquired with  $E \parallel a_m$  ( $a_m$  being the  $a$ -axis of the monoclinic insulator lattice).  $a_m$  and  $c_r$  were directed along the same spatial direction so as to also be in the insulating phase where we were maximizing the signal coming from the  $d_{\parallel}$  band.

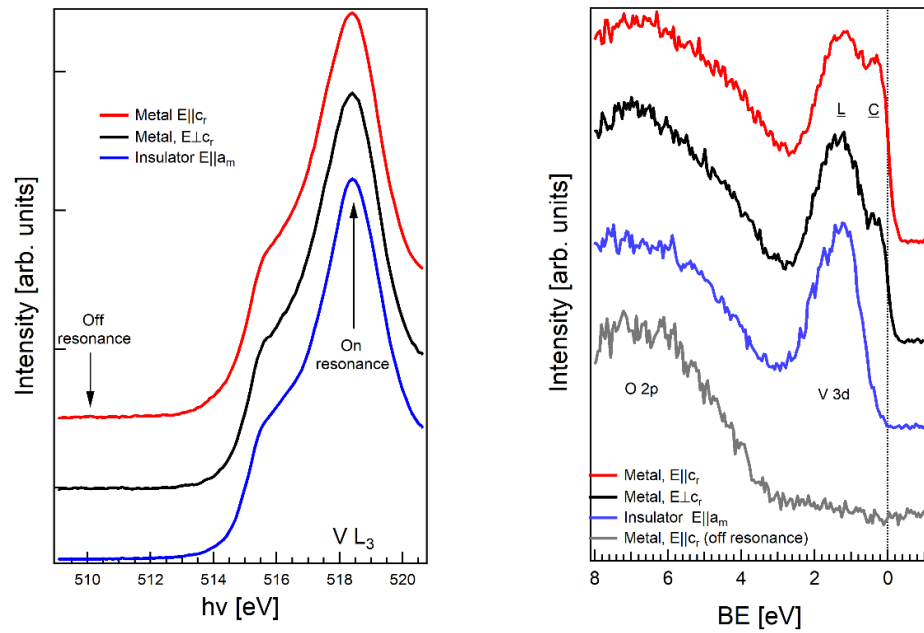


**Figure 3.** (Left): XAS spectra of the V L<sub>3</sub> edge acquired for the metal and insulator phases. The spectra are vertically shifted for clarity. (Right): ResPES spectra acquired off resonance and on resonance (as depicted in the right panel) for different sample orientations. The spectra were normalized to the O 2p peak and vertically shifted for clarity. In the insulator phase the lattice of VO<sub>2</sub> has monoclinic symmetry and the electric field E is parallel to the a axis (a<sub>m</sub>). The insulated monoclinic a axis and the metallic rutile c axis are oriented along the same direction; in addition, in the insulating phase we probed mostly the d<sub>||</sub> band.

The metallic spectra acquired on resonance showed a two-peaked structure corresponding to the V 3d unpaired electrons.

These two peaks were generated by two different screening channels in the valence band of VO<sub>2</sub> [51]. The feature centered around 1.7 eV was called the ligand hole (L) and accounted for the local screening of the photo-induced hole by an O 2p electron. The peak at about 0.4–0.5 eV was named the coherent hole (C) and generated by the non-local screening of the photo-hole from V 3d electrons that were free to move in the solid and were, therefore, the final state effect.

It is evident that C was more intense when the electric field was oriented parallel to the c<sub>r</sub> axis; this suggests that the d<sub>||</sub> was more populated with respect to π\* pointing out the anisotropic electron population of these bands. To quantify the anisotropy in the sample, we adopted the same approach proposed in reference [41] to calculate the ratio between the screening length in the insulating phase and in the metallic phase for both the electric field orientation. For a ResPES spectrum, the relation between intensity and the screening length was the following [52–54].

$$\frac{I}{I_0} \propto \lambda \tag{1}$$

where I is the ResPES spectrum intensity, I<sub>0</sub> is the incident photon flux, and λ is the screening length. The ratio  $\frac{\lambda_m}{\lambda_i}$  (where λ<sub>m</sub> is the screening length for the metallic phase while λ<sub>i</sub> for the insulating phase) could, therefore, be calculated by integrating the ResPES spectra between 0 and 2 eV. The selection of the energy interval 0–2 eV to calculate λ is arbitrary. The only two requirements we followed were to include both the L and C in the integrated region and to minimize the tail coming from the O 2p feature centered at 7 eV. The numerical results did not change significantly if we slightly changed the interval of integration.

The results for  $\frac{\lambda_m}{\lambda_i}$  are reported in Table 1.  $\lambda_m$  were calculated with  $E \parallel c_r$ , and  $E \perp c_r$ , while  $\lambda_i$  was calculating using the insulating spectrum reported in Figure 3's right panel with  $E \parallel a_m$ .

**Table 1.**  $\lambda_m/\lambda_i$  calculated for the two configurations  $E \parallel c_r$  and  $E \perp c_r$ .

	$E \parallel c_r (d_{  })$	$E \perp c_r (\pi^*)$
$\lambda_m/\lambda_i$	0.418	0.502

The difference between the two sample orientations is evident: when  $E \parallel c_r$ ,  $\lambda_m/\lambda_i$  was ~20% smaller with respect to  $E \perp c_r$ . This is a direct probe of the intrinsic anisotropy of the VO<sub>2</sub> band structure and the measurement of the different screening capabilities of  $d_{||}$  and  $\pi^*$  bands.

These preliminary results show the importance of using a band selective probe to study a complex problem such as the VO<sub>2</sub> MIT and that this approach was fundamental in order to accurately take into account the anisotropy degree of freedom.

#### 4. Conclusions

We show our preliminary results obtained by studying a sample of a single crystalline VO<sub>2</sub>/TiO<sub>2</sub>(101) film of an 8 nm thickness. This film is of extremely good quality. The resistivity measurements show a hysteretic behavior with a critical temperature of 321 K, a transition width of 8.2 K, and a jump in resistivity of ~3 orders of magnitude. XRD measurements show that the residual compressive strain imposed by the epitaxial growth was ~0.8%. We investigated the intrinsic band anisotropy of metallic VO<sub>2</sub> by using ResPES at the V L<sub>3</sub> edge with linearly polarized light. The combined access to resonantly enhanced the photoelectron yield and the bands' selectivity allowed us to discriminate between the  $d_{||}$  and  $\pi^*$  bands' contribution at FL. This unique approach allowed our experimental investigation to obtain new insight into the VO<sub>2</sub> band structure with respect to previous studies [4,20]. We observed that the ratio between the screening length of the metallic and insulating phase ( $\lambda_m/\lambda_i$ ) for  $d_{||}$  and  $\pi^*$  bands differed by about 20%, pointing out a strongly anisotropic screening capability in VO<sub>2</sub>. Since the difference in the electron population between the  $d_{||}$  and  $\pi^*$  bands was a key parameter to controlling the MIT properties, our preliminary results highlight the importance of using a resonantly enhanced band selective spectroscopic tool to study complex systems such as VO<sub>2</sub>.

**Author Contributions:** A.D., Conceptualization; A.D., V.P. and A.Y.P., Data curation; A.D., V.P. and A.Y.P., Formal analysis; A.D. Supervision; A.D. Validation; A.D., J.R. and V.P. Visualization; V.P. and A.Y.P. Investigation; L.L., C.Z. and A.M. Resources; A.D., Writing—original draft; A.D., V.P., A.Y.P., L.L., C.Z., J.R. and A.M. All authors have read and agreed to the published version of the manuscript.

**Funding:** This work was partially performed in the framework of the Nanoscience Foundry and Fine Analysis (NFFA-MUR Italy Progetti Internazionali) project ([www.trieste.NFFA.eu](http://www.trieste.NFFA.eu)).

**Data Availability Statement:** Data available on request. The data presented in this study are available on request from the corresponding author.

**Conflicts of Interest:** The authors declare no conflict of interest.

## Appendix A

### Resonant Photoemission

ResPES is a branch of variable energy photoemission spectroscopy. Using synchrotron facilities, it is possible to vary the photon energy across the photo-absorption resonance of the system, thus exploiting cross-section effects to enhance specific photoemission features. ResPES was realized when the photon energy was tuned to match the absorption edge of one of the elements present at the surface of the sample. In this case, two possible pathways that lead to the same final state were possible: the direct photoemission and the Auger-like

emission that followed the relaxation of a photo-excited state. An interference process took place and enhanced the spectral intensity of the resonating states as a function of the photon energy.

Tuning the photon energy across the VO<sub>2</sub> L<sub>3</sub> edge, a 2*p* electron was excited in the empty 3*d* band. This excited state decays via an Auger-like process, with a concurrent emission of a photo-electron. This process is represented in Figure A1.

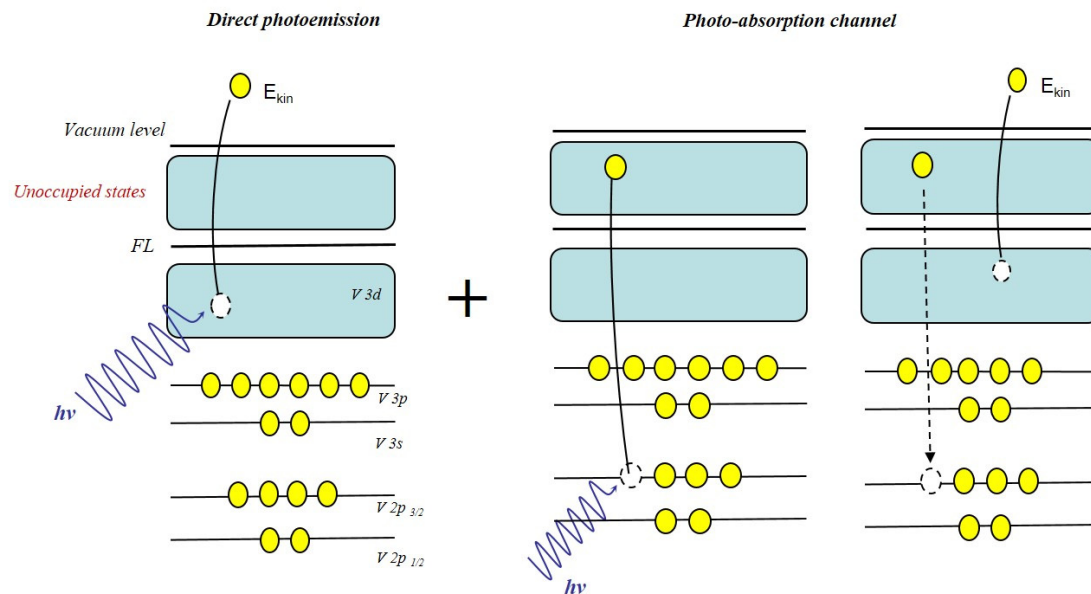
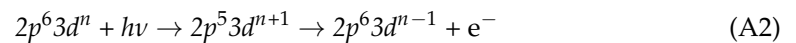


**Figure A1.** Schematic representation of the two concurrent photoemission channels that lead to the resonant enhancement of V 3*d* electrons. **(Left):** A direct photoemission channel with the excitation of a V 3*d* electron above the vacuum level. **(Right):** Photo-absorption channel. An electron from the V 2*p*<sub>3/2</sub> core level is excited into an unoccupied state. This unstable state decays through an Auger-like process leading to the same final state as in the direct photoemission channel.

The two identical final states are reported in Equations (A1) and (A2). This includes direct photoemission channel:



and the photo-absorption channel:



The coherent superposition of channels in Equations (A1) and (A2) led to the resonant enhancement of the 3*d*<sup>*n*−1</sup> final state [55]. Since the V 3*d* electrons were those involved in the VO<sub>2</sub> MIT, the capability to enhance their signal above the background is of great importance.

## References

1. Fisher, B.; Genossar, J.; Reisner, G. Systematics in the metal-insulator transition temperatures in vanadium oxides. *Solid State Commun.* **2016**, *226*, 29–32. [CrossRef]
2. Eyert, V. The metal-insulator transitions of VO<sub>2</sub>: A band theoretical approach. *Ann. Phys.* **2002**, *11*, 650–704. [CrossRef]
3. Demeter, M.; Neumann, M.; Reichelt, W. Mixed-valence vanadium oxides studied by XPS. *Surf. Sci.* **2000**, *454*, 41–44. [CrossRef]
4. Shin, S.; Suga, S.; Taniguchi, M.; Fujisawa, M.; Kanzaki, H.; Fujimori, A.; Daimon, H.; Ueda, Y.; Kosuge, K.; Kachi, S. Vacuum-ultraviolet reflectance and photoemission study of the metal-insulator phase transitions in VO<sub>2</sub>, V<sub>6</sub>O<sub>13</sub>, and V<sub>2</sub>O<sub>3</sub>. *Phys. Rev. B* **1990**, *41*, 4993–5009. [CrossRef]
5. Haverkort, M.W.; Hu, Z.; Tanaka, A.; Reichelt, W.; Streltsov, S.V.; Korotin, M.A.; Anisimov, V.I.; Hsieh, H.H.; Lin, H.-J.; Chen, C.T.; et al. Orbital-Assisted Metal-Insulator Transition in VO<sub>2</sub>. *Phys. Rev. Lett.* **2005**, *95*, 196404. [CrossRef]

6. Polewczyk, V.; Chaluvadi, S.; Dagur, D.; Mazzola, F.; Chalil, S.P.; Petrov, A.; Fujii, J.; Panaccione, G.; Rossi, G.; Orgiani, P.; et al. Chemical, structural and electronic properties of ultrathin  $V_2O_3$  films on  $Al_2O_3$  substrate: Implications in Mott-like transitions. *Appl. Surf. Sci.* **2023**, *610*, 155462. [[CrossRef](#)]
7. D'Elia, A.; Rezvani, S.J.; Zema, N.; Zuccaro, F.; Fanetti, M.; Belec, B.; Li, B.W.; Zou, C.W.; Spezzani, C.; Sacchi, M.; et al. Stoichiometry and disorder influence over electronic structure in nanostructured  $VO_x$  films. *J. Nanoparticle Res.* **2021**, *23*, 33. [[CrossRef](#)]
8. Fu, D.; Liu, K.; Tao, T.; Lo, K.; Cheng, C.; Liu, B.; Zhang, R.; Bechtel, H.A.; Wu, J. Comprehensive study of the metal-insulator transition in pulsed laser deposited epitaxial  $VO_2$  thin films. *J. Appl. Phys.* **2013**, *113*, 043707. [[CrossRef](#)]
9. Fan, L.L.; Chen, S.; Luo, Z.L.; Liu, Q.H.; Wu, Y.F.; Song, L.; Ji, D.X.; Wang, P.; Chu, W.S.; Gao, C.; et al. Strain Dynamics of Ultrathin  $VO_2$  Film Grown on  $TiO_2$  (001) and the Associated Phase Transition Modulation. *Nano Lett.* **2014**, *14*, 4036–4043. [[CrossRef](#)]
10. Cui, Y.; Ke, Y.; Liu, C.; Chen, Z.; Wang, N.; Zhang, L.; Zhou, Y.; Wang, S.; Gao, Y.; Long, Y. Thermochromic  $VO_2$  for Energy-Efficient Smart Windows. *Joule* **2018**, *2*, 1707–1746. [[CrossRef](#)]
11. Chen, S.; Wang, Z.; Ren, H.; Chen, Y.; Yan, W.; Wang, C.; Li, B.; Jiang, J.; Zou, C. Gate-controlled  $VO_2$  phase transition for high-performance smart windows. *Sci. Adv.* **2019**, *5*, eaav6815. [[CrossRef](#)]
12. Kang, C.; Zhang, C.; Yao, Y.; Yang, Y.; Zong, H.; Zhang, L.; Li, M. Enhanced Thermochromic Properties of Vanadium Dioxide ( $VO_2$ )/Glass Heterostructure by Inserting a Zr-Based Thin Film Metallic Glasses ( $Cu_{50}Zr_{50}$ ) Buffer Layer. *Appl. Sci.* **2018**, *8*, 1751. [[CrossRef](#)]
13. Lin, J.; Ramanathan, S.; Guha, S. Electrically Driven Insulator–Metal Transition-Based Devices—Part I: The Electrothermal Model and Experimental Analysis for the DC Characteristics. *IEEE Trans. Electron. Devices* **2018**, *65*, 3982–3988. [[CrossRef](#)]
14. Ramanathan, S. *Thin Film Metal-Oxides: Fundamentals and Applications in Electronics and Energy*; Springer: Boston, MA, USA, 2010. [[CrossRef](#)]
15. Brahlek, M.; Zhang, L.; Lapano, J.; Zhang, H.-T.; Engel-Herbert, R.; Shukla, N.; Datta, S.; Paik, H.; Schlom, D.G. Opportunities in vanadium-based strongly correlated electron systems. *MRS Commun.* **2017**, *7*, 27–52. [[CrossRef](#)]
16. Zimmermann, R.; Claessen, R.; Reinert, F.; Steiner, P.; Hüfner, S. Strong hybridization in vanadium oxides: Evidence from photoemission and absorption spectroscopy. *J. Phys. Condens. Matter* **1998**, *10*, 5697–5716. [[CrossRef](#)]
17. Qazilbash, M.M.; Burch, K.; Whisler, D.; Shrekenhamer, D.; Chae, B.G.; Kim, H.T.; Basov, D.N. Correlated metallic state of vanadium dioxide. *Phys. Rev. B Condens. Matter Mater. Phys.* **2006**, *74*, 205118. [[CrossRef](#)]
18. Weber, C.; O'regan, D.D.; Hine, N.D.M.; Payne, M.C.; Kotliar, G.; Littlewood, P.B. Vanadium Dioxide: A Peierls-Mott Insulator Stable against Disorder. *Phys. Rev. Lett.* **2012**, *108*, 256402. [[CrossRef](#)]
19. Zylbersztejn, A.; Mott, N.F. Metal-insulator transition in vanadium dioxide. *Phys. Rev. B* **1975**, *11*, 4383–4395. [[CrossRef](#)]
20. Koethe, T.C.; Hu, Z.; Haverkort, M.W.; Schüßler-Langeheine, C.; Venturini, F.; Brookes, N.B.; Tjernberg, O.; Reichelt, W.; Hsieh, H.H.; Lin, H.-J.; et al. Transfer of Spectral Weight and Symmetry across the Metal-Insulator Transition in  $VO_2$ . *Phys. Rev. Lett.* **2006**, *97*, 116402. [[CrossRef](#)]
21. D'Elia, A.; Grazioli, C.; Cossaro, A.; Li, B.W.; Zou, C.W.; Rezvani, S.J.; Pinto, N.; Marcelli, A.; Coreno, M. Electron Correlation driven Metal-Insulator transition in Strained and Disordered  $VO_2$  films. *arXiv* **2020**, arXiv:2006.07930.
22. Singh, C.N.; Piper, L.F.J.; Paik, H.; Schlom, D.G.; Lee, W.-C. Correlation-induced emergent charge order in metallic vanadium dioxide. *arXiv* **2020**, arXiv:2005.02957. [[CrossRef](#)]
23. Aetukuri, N.B.; Gray, A.X.; Drouard, M.; Cossale, M.; Gao, L.; Reid, A.H.; Kukreja, R.; Ohldag, H.; Jenkins, C.A.; Arenholz, E.; et al. Control of the metal-insulator transition in vanadium dioxide by modifying orbital occupancy. *Nat. Phys.* **2013**, *9*, 661–666. [[CrossRef](#)]
24. Natelson, D. Condensed-matter physics: A solid triple point. *Nature* **2013**, *500*, 408–409. [[CrossRef](#)] [[PubMed](#)]
25. Tricoire, M.; Mahieu, N.; Simler, T.; Nocton, G. Intermediate Valence States in Lanthanide Compounds. *Chem. A Eur. J.* **2021**, *27*, 6860–6879. [[CrossRef](#)] [[PubMed](#)]
26. Pruessmann, T.; Nagel, P.; Simonelli, L.; Batchelor, D.; Gordon, R.; Schimmelpfennig, B.; Trumm, M.; Vitova, T. Opportunities and challenges of applying advanced X-ray spectroscopy to actinide and lanthanide N-donor ligand systems. *J. Synchrotron. Radiat.* **2022**, *29*, 53–66. [[CrossRef](#)] [[PubMed](#)]
27. Bianconi, A.; Marcelli, A.; Dexpert, H.; Karnatak, R.; Kotani, A.; Jo, T.; Petiau, J. Specific intermediate-valence state of insulating 4f compounds detected by  $L_3$  X-ray absorption. *Phys. Rev. B* **1987**, *35*, 806–812. [[CrossRef](#)]
28. Bianconi, A. Multiplet splitting of final-state configurations in X-ray-absorption spectrum of metal  $VO_2$ : Effect of core-hole-screening, electron correlation, and metal-insulator transition. *Phys. Rev. B* **1982**, *26*, 2741–2747. [[CrossRef](#)]
29. Gray, A.X.; Jeong, J.; Aetukuri, N.P.; Granitzka, P.; Chen, Z.; Kukreja, R.; Higley, D.; Chase, T.; Reid, A.H.; Ohldag, H.; et al. Correlation-Driven Insulator-Metal Transition in Near-Ideal Vanadium Dioxide Films. *Phys. Rev. Lett.* **2016**, *116*, 116403. [[CrossRef](#)]
30. Paez, G.J.; Singh, C.N.; Wahila, M.J.; Tirpak, K.E.; Quackenbush, N.F.; Sallis, S.; Paik, H.; Liang, Y.; Schlom, D.G.; Lee, T.-L.; et al. Simultaneous Structural and Electronic Transitions in Epitaxial  $VO_2/TiO_2(001)$ . *Phys. Rev. Lett.* **2020**, *124*, 196402. [[CrossRef](#)]
31. Mukherjee, S.; Quackenbush, N.F.; Paik, H.; Schlueter, C.; Lee, T.-L.; Schlom, D.G.; Piper, L.F.J.; Lee, W.-C. Tuning a strain-induced orbital selective Mott transition in epitaxial  $VO_2$ . *Phys. Rev. B* **2016**, *93*, 241110. [[CrossRef](#)]
32. Evlyukhin, E.; Howard, S.A.; Paik, H.; Paez, G.J.; Gosztola, D.J.; Singh, C.N.; Schlom, D.G.; Lee, W.-C.; Piper, L.F.J. Directly measuring the structural transition pathways of strain-engineered  $VO_2$  thin films. *Nanoscale* **2020**, *12*, 18857–18863. [[CrossRef](#)]

33. D'Elia, A.; Grazioli, C.; Cossaro, A.; Li, B.; Zou, C.; Rezvani, S.J.; Marcelli, A.; Coreno, M. Detection of Spin Polarized Band in VO<sub>2</sub>/TiO<sub>2</sub>(001) Strained Films via Orbital Selective Constant Initial State Spectroscopy. *Condens. Matter* **2020**, *5*, 72. [[CrossRef](#)]
34. D'Elia, A.; Rezvani, S.; Cossaro, A.; Stredansky, M.; Grazioli, C.; Li, B.W.; Zou, C.; Coreno, M.; Marcelli, A. Strain Induced Orbital Dynamics Across the Metal Insulator Transition in Thin VO<sub>2</sub>/TiO<sub>2</sub> (001) Films. *J. Supercond. Nov. Magn.* **2020**, *33*, 2383–2388. [[CrossRef](#)]
35. Mondal, D.; Mahapatra, S.R.; Ahmed, T.; Podapangi, S.K.; Ghosh, A.; Aetukuri, N.P.B. Atomically-smooth single-crystalline VO<sub>2</sub> (101) thin films with sharp metal-insulator transition. *J. Appl. Phys.* **2019**, *126*, 215302. [[CrossRef](#)]
36. Lu, J.; West, K.G.; Wolf, S.A. Very large anisotropy in the dc conductivity of epitaxial VO<sub>2</sub> thin films grown on (011) rutile TiO<sub>2</sub> substrates. *Appl. Phys. Lett.* **2008**, *93*, 262107. [[CrossRef](#)]
37. Kittiwatanakul, S.; Lu, J.; Wolf, S.A. Transport Anisotropy of Epitaxial VO<sub>2</sub> Films near the Metal–Semiconductor Transition. *Appl. Phys. Express* **2011**, *4*, 091104. [[CrossRef](#)]
38. Lee, S.; Hippalgaonkar, K.; Yang, F.; Hong, J.; Ko, C.; Suh, J.; Liu, K.; Wang, K.; Urban, J.J.; Zhang, X.; et al. Anomalously low electronic thermal conductivity in metallic vanadium dioxide. *Science* **2017**, *355*, 371–374. [[CrossRef](#)]
39. Bongers, P. Anisotropy of the electrical conductivity of VO<sub>2</sub> single crystals. *Solid State Commun.* **1965**, *3*, 275–277. [[CrossRef](#)]
40. Goodenough, J.B. The two components of the crystallographic transition in VO<sub>2</sub>. *J. Solid State Chem.* **1971**, *3*, 490–500. [[CrossRef](#)]
41. D'Elia, A.; Grazioli, C.; Cossaro, A.; Li, B.; Zou, C.; Rezvani, S.; Pinto, N.; Marcelli, A.; Coreno, M. Strain mediated Filling Control nature of the Metal-Insulator Transition of VO<sub>2</sub> and electron correlation effects in nanostructured films. *Appl. Surf. Sci.* **2020**, *540*, 148341. [[CrossRef](#)]
42. Fan, L.L.; Chen, S.; Liao, G.M.; Chen, Y.L.; Ren, H.; Zou, C.W. Comprehensive studies of interfacial strain and oxygen vacancy on metal–insulator transition of VO<sub>2</sub> film. *J. Phys. Condens. Matter* **2016**, *28*, 255002. [[CrossRef](#)] [[PubMed](#)]
43. Marcelli, A.; Coreno, M.; Stredansky, M.; Xu, W.; Zou, C.; Fan, L.; Chu, W.; Wei, S.; Cossaro, A.; Ricci, A.; et al. Nanoscale Phase Separation and Lattice Complexity in VO<sub>2</sub>: The Metal–Insulator Transition Investigated by XANES via Auger Electron Yield at the Vanadium L23-Edge and Resonant Photoemission. *Condens. Matter* **2017**, *2*, 38. [[CrossRef](#)]
44. Laverock, J.; Preston, A.R.H.; Newby, J.D.; Smith, K.E.; Sallis, S.; Piper, L.F.J.; Kittiwatanakul, S.; Lu, J.W.; Wolf, S.A.; Leandersson, M.; et al. Photoemission evidence for crossover from Peierls-like to Mott-like transition in highly strained VO<sub>2</sub>. *Phys. Rev. B Condens. Matter Mater. Phys.* **2012**, *86*, 195124. [[CrossRef](#)]
45. Fan, L.L.; Chen, S.; Wu, Y.F.; Chen, F.H.; Chu, W.S.; Chen, X.; Zou, C.W.; Wu, Z.Y. Growth and phase transition characteristics of pure M-phase VO<sub>2</sub> epitaxial film prepared by oxide molecular beam epitaxy. *Appl. Phys. Lett.* **2013**, *103*, 131914. [[CrossRef](#)]
46. Panaccione, G.; Vobornik, I.; Fujii, J.; Krizmancic, D.; Annese, E.; Giovanelli, L.; Maccherozzi, F.; Salvador, F.; De Luisa, A.; Benedetti, D.; et al. Advanced photoelectric effect experiment beamline at Elettra: A surface science laboratory coupled with Synchrotron Radiation. *Rev. Sci. Instrum.* **2009**, *80*, 043105. [[CrossRef](#)]
47. Stöhr, J. Principles, Techniques, and Instrumentation of NEXAFS. *NEXAFS Spectrosc.* **1992**, *25*, 114–161. [[CrossRef](#)]
48. Kittiwatanakul, S.; Wolf, S.A.; Lu, J. Large epitaxial bi-axial strain induces a Mott-like phase transition in VO<sub>2</sub>. *Appl. Phys. Lett.* **2014**, *105*, 073112. [[CrossRef](#)]
49. Eguchi, R.; Taguchi, M.; Matsunami, M.; Horiba, K.; Yamamoto, K.; Ishida, Y.; Chainani, A.; Takata, Y.; Yabashi, M.; Miwa, D.; et al. Photoemission evidence for a Mott–Hubbard metal-insulator transition in VO<sub>2</sub>. *Phys. Rev. B Condens. Matter Mater. Phys.* **2008**, *78*, 075115. [[CrossRef](#)]
50. D'Elia, A.; Cepek, C.; de Simone, M.; Macis, S.; Belec, B.; Fanetti, M.; Piseri, P.; Marcelli, A.; Coreno, M. Interplay among work function, electronic structure and stoichiometry in nanostructured VO<sub>x</sub> films. *Phys. Chem. Chem. Phys.* **2020**, *22*, 6282–6290. [[CrossRef](#)]
51. Mossaneck, R.J.O.; Abbate, M. Cluster model calculations with nonlocal screening channels of metallic and insulating VO<sub>2</sub>. *Phys. Rev. B Condens. Matter Mater. Phys.* **2006**, *74*, 125112. [[CrossRef](#)]
52. Dowben, P. The metallicity of thin films and overlayers. *Surf. Sci. Rep.* **2000**, *40*, 151–247. [[CrossRef](#)]
53. McIlroy, D.N.; Waldfried, C.; Zhang, J.; Choi, J.-W.; Foong, F.; Liou, S.H.; Dowben, P.A. Comparison of the temperature-dependent electronic structure of the perovskites. *Phys. Rev. B Condens. Matter Mater. Phys.* **1996**, *54*, 17438–17451. [[CrossRef](#)]
54. Li, D.; Zhang, J.; Lee, S.; Dowben, P.A. Evidence for the formation of metallic mercury overlayers on Si(111). *Phys. Rev. B* **1992**, *45*, 11876–11884. [[CrossRef](#)]
55. Tanaka, A.; Jo, T. Resonant 3d, 3p and 3s Photoemission in Transition Metal Oxides Predicted at 2p Threshold. *J. Phys. Soc. Jpn.* **1994**, *63*, 2788–2807. [[CrossRef](#)]

**Disclaimer/Publisher's Note:** The statements, opinions and data contained in all publications are solely those of the individual author(s) and contributor(s) and not of MDPI and/or the editor(s). MDPI and/or the editor(s) disclaim responsibility for any injury to people or property resulting from any ideas, methods, instructions or products referred to in the content.